BIOCHEMISTRY
including biophysical chemistry & molecular biology

Article

pubs.acs.org/biochemistry

Identification of Function and Mechanistic Insights of Guanine Deaminase from *Nitrosomonas europaea*: Role of the C-Terminal Loop in Catalysis

Aruna Bitra, Bhukya Hussain,[†,‡] Ajay Singh Tanwar,[‡] and Ruchi Anand*

Department of Chemistry, IIT Bombay, Mumbai, India 400076

Supporting Information

ABSTRACT: NE0047 from *Nitrosomonas europaea* has been annotated as a zinc-dependent deaminase; however, the substrate specificity is unknown because of the low level of structural similarity and sequence identity compared to other family members. In this study, the function of NE0047 was established as a guanine deaminase (catalytic efficiency of 1.2×10^5 M^{-1} s^{-1}), exhibiting secondary activity towards ammeline. The structure of NE0047 in the presence of the substrate analogue 8-azaguanine was also determined to a resolution of 1.9 Å. NE0047 crystallized as a homodimer in an asymmetric unit. It was found that the extreme nine-amino acid C-terminal loop forms an active site flap; in one monomer, the flap is in the closed conformation and in the other in the open conformation with this loop region exposed to the solvent. Calorimetric data obtained using the full-length version of the enzyme fit to a sequential binding model, thus supporting a cooperative mode of ligand occupancy. In contrast, the mutant form of the enzyme (ΔC) with the deletion of the extreme nine amino acids follows an independent model of ligand occupancy. In addition, the ΔC mutant also does not exhibit any enzyme activity. Therefore, we propose that the progress of the reaction is communicated via changes in the conformation of the C-terminal flap and the closed form of the enzyme is the catalytically active form, while the open form allows for product release. The catalytic mechanism of deamination was also investigated, and we found that the mutagenesis of the highly conserved active site residues Glu79 and Glu143 resulted in a complete loss of activity and concluded that they facilitate the reaction by serving as proton shuttles.

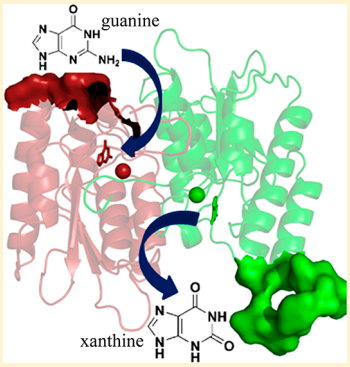

Nucleobase deamination is a highly versatile reaction that is used in various facets of biology. The enzymes serve as regulators of the total cellular purine and pyrimidine derivative pool and are key enzymes involved in nucleotide catabolism, a pathway that provides both nitrogen and carbon sources in organisms.[1] Defects in purine metabolism can be lethal as they may lead to incorporation of deaminated bases like hypoxanthine and xanthine into the DNA architecture, leading to miscoding and interference with RNA editing and function.[2] In addition, tRNA editing deaminases employ posttranslational deamination of cytidine and adenosine bases to enhance the repertoire of codon usage by introducing base pair flexibility at the wobble position of a single tRNA.[3] Organisms thus maintain stringent control on the level of the nucleobase derivative pool for proper functioning. Nucleobase deaminases can also serve as attractive drug targets. For instance, mammalian guanine deaminases (GD) can be used in this respect as they are expressed differentially in a tissue specific manner[4,5] and serve as specific markers for the onset of liver-related diseases and in the development of neuronal morphology.[5,6]

There are two well-studied nucleobase deaminase families: (1) the amidohydrolase superfamily (AHS) and (2) the cytidine deaminase (CDA) superfamily. Both families use metal-assisted deamination as the primary mode of catalysis. However, they show extreme sequence and structural divergence. The AHS deaminases have a distorted triosephosphate isomerase fold and in some cases contain multiple metal centers.[7,8] The CDA superfamily members have a relatively compact $\alpha\beta\alpha$ layered fold and are reported to use only zinc for deamination. All CDA superfamily members contain a ubiquitous metal binding signature HXE and PCXXC,[9,10] which is a hallmark of this family.

Because of the importance of nucleobase deaminases in biology, a major thrust in this field has been the identification of these novel enzymes.[11,12] With the increased number of genome sequencing projects underway, the curation of genes encoded by various organisms is growing exponentially. As a byproduct of this enhanced databank of information, one of the most important emerging challenges is to predict the function of a protein that a gene encodes.[13−15] Statistics reveal that for a model set of 37 well-studied protein families, 40% of the sequences deposited as of 2005 were misannotated.[16] Therefore, decrypting the exact function of a particular enzyme is considered to be a daunting task.[17] This is mostly because in several instances the query in question has a low level of sequence homology with other members of the family to which it is speculatively annotated, and hence, it is difficult to make an

Received: January 18, 2013
Revised: April 2, 2013
Published: April 4, 2013

inference of the exact function solely on the basis of comparison of primary sequences. An alternative approach to deciphering the function of the protein with unknown activity is to use structure-based prediction methods.[18−20] This approach when combined with existing bioinformatics tools can be an extremely powerful method for solving this seemingly insurmountable problem.[18,21−23] However, structure-based activity prediction also poses its own set of constrains. It becomes challenging to assign function when enzymes catalyze more than one type of reaction with varying degrees of efficiency, as observed in the serine protease superfamily.[24] In addition, for any potential substrate, a series of possible analogues with the same functional group can be accommodated in the active site, resulting in ambiguity in assigning the exact function.[25]

For this study, we selected an enzyme of known structure but unknown substrate specificity, NE0047 from *Nitrosomonas europaea* (PDB entry 2G84), which has been formally assigned to the CDA superfamily. The following questions were addressed. (1) What is the identity of the nucleobase deaminated by NE0047? (2) How does a particular nucleobase deaminase differentiate between substrates while maintaining fidelity of function? (3) What are the conformational changes required to facilitate the reaction? (4) What is the molecular mechanism of nucleobase deamination?

An initial expansive sequence analysis approach using all the members of the clusters of orthologous group (COG), cog0590 to which NE0047 belongs, failed to decipher the exact reaction catalyzed by it (Figure 1). This was mostly because NE0047 shares a low level of sequence similarity with other members of the CDA superfamily, typically in the range of 20−30%. Hence, a combination of computational and experimental tools was required to identify the function of NE0047. Here, we show that NE0047 primarily catalyzes the deamination of guanine to xanthine, and also surprisingly enough, we found that it exhibits secondary activity toward deamination of ammeline. In addition, using an amalgamation of structural and biochemical studies, we have been able to provide new insights into the mechanism of nucleobase deamination, in particular toward the conformational changes that occur during the course of the reaction. Furthermore, the molecular mechanism of deamination was also probed, and residues important for catalysis were identified.

MATERIALS AND METHODS

Expression and Purification of NE0047. The NE0047 plasmid was a gift from the Midwest Center for Structural Genomics Consortium (Toronto, ON). All the mutants of NE0047 were made with the site-directed mutagenesis kit from Kapa biosystems. The native NE0047 (residues 1−192), the form of NE0047 with the extreme 12 C-terminal residues deleted [ΔC(1−180)], and other mutants were expressed as six-His tag fusion proteins to facilitate purification, after which the tag was proteolytically removed. The protein was expressed in *Escherichia coli* BL21(DE3) cells and purified using Qiagen Ni-NTA resin. The bound NE0047 protein was eluted with 100 mM imidazole. The His tag was removed from the protein by overnight cleavage with tobacco etch virus (TEV) protease at a molar ratio of 1:40. The His tag cleaved protein was further purified by size exclusion chromatography using a Superdex 75 column in 20 mM HEPES (pH 7.5) and 100 mM NaCl. The protein fractions from the column were pooled together and concentrated to 10 mg/mL, flash-frozen in liquid N_2, and stored at −80 °C until they were used.

Docking Studies. The 1.4 Å X-ray structure of NE0047 was downloaded from the PDB, and its monomer was used for docking calculations. All docking runs were conducted by using a genetic algorithm (GA) in AutoDock version 4.2[26] against different ligands. The active site metal ion was assigned a charge of +2. Each ligand was scored according to a free energy cost function (ΔG^*) that accounts for van der Waals, hydrogen bonding, electrostatic, solvation, and torsional free energy terms. The grid box for docking was selected in the active site region, and rigid docking was performed with 150 runs for each ligand. On the basis of the estimated free energy of binding (ΔG^*) calculated in docking, the top-ranked metabolites were selected to test activity.

Measurement of Enzymatic Activity. The activity screening of a variety of substrates and the measurement of kinetic constants for the deamination of guanine and its analogues were conducted using the Berthelot reaction[27] and monitored spectrophotometrically at 630 nm. The concentrations of the enzyme and each substrate were 4 and 250 μM, respectively, and the incubation time was 10 min. The compounds tested for activity assay included (**1**) guanine, (**2**) 8-azaguanine, (**3**) ammeline, (**4**) 6-thioguanine, (**5**) adenine, (**6**) cytosine, (**7**) 1-methylguanine, (**8**) hypoxanthine, (**9**) 2,6-diaminopurine, (**10**) 2-amino-6-chloropurine, (**11**) 9-methylguanine, (**12**) adenosine, (**13**) guanosine, (**14**) cytidine, (**15**) 2′-deoxyguanosine, (**16**) AMP, (**17**) GMP, (**18**) 2′-deoxyGMP, (**19**) CMP, and (**20**) 2′-deoxyCMP.

Enzyme kinetics were performed by first incubating 230 nM purified enzyme in 200 μL of phosphate buffer (pH 7.5) with different concentrations (30−200 μM) of substrate at 37 °C for 10 min and then quenching with 40 μL of 0.67 N H_2SO_4 and 20 μL of 10% (w/v) sodium tungstate. The liberated ammonia reacts with phenol color reagent and alkaline hypochlorite to give a blue color that was measured spectrophotometrically at 630 nm.[27] All the kinetic parameters were obtained by fitting the data in the following Michaelis−Menten equation in SigmaPlot.

Structure Determination. Two crystal structures were reported: NE0047 complexed with 8-azagaunine (PDB entry 4HRQ) and NE0047 (E79A) complexed with 8-azaguanine (PDB entry 4HRW). All these crystals were grown by the hanging drop vapor diffusion method at 18 °C by mixing 2 μL of the protein solution [0.5 M NaCl, 10 mM HEPES (pH 7.6), 2 mM L-cysteine, and 10 mM 8-azaguanine] and 1 μL of the reservoir solution (0.225 M $MgCl_2$, 25% PEG 3350, and 0.1 M Bis-Tris) and equilibrating against 1 mL of the reservoir solution. The crystals were cryo-protected with a solution composed of mother liquor combined with 5% glycerol, 5% sucrose, and 5% ethylene glycol and flash-cooled in liquid nitrogen. The X-ray diffraction data for the NE0047−8-azaguanine complex were collected at beamline BM-14 at European Synchrotron Radiation Facility (ESRF, Grenoble, France) using a MAR CCD detector, 1° oscillation, a 8 s exposure time, and a crystal−detector distance of 142 mm. The X-ray diffraction data for the NE0047 (E79A)−8-azaguanine complex were collected at the National Institute of Immunology (Delhi, India) using a RAXIS IV++ image plate detector, 1° oscillation, a 5 min exposure time, and a crystal−detector distance of 200 mm.

The data were indexed, integrated, and scaled using iMOSFLM[28] and CCP4.[29] All crystals belong to orthorhombic

dx.doi.org/10.1021/bi400068g | *Biochemistry* 2013, 52, 3512−3522

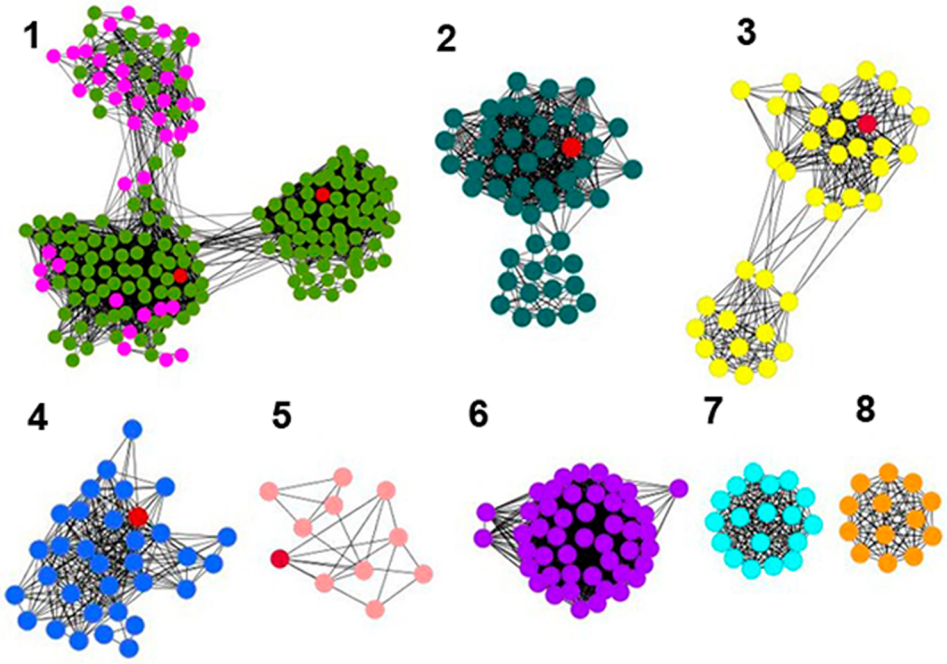

Figure 1. Sequence similarity network of cog0590 at a BLASTP cutoff of e^{-40}. In each group, the nodes represent the proteins and the edges the BLASTP linkages. The length of edges is not significant except for the tightly clustered groups. In each group, the proteins with crystal structures available are colored red. The representative crystal structures were tRNA adenosine deaminase from *Staphylococcus aureus* (PDB entry 2B3J) and *E. coli* (PDB entry 1Z3A) in group 1, *Bacillus subtilis* guanine deaminase (PDB entry 1WKQ) in group 2, *Saccharomyces cerevisiae* cytosine deaminase (PDB entry 1UAQ) in group 3, and cytidine/deoxycytidylate deaminase from *Agrobacterium tumefaciens* (PDB entry 2A8N) in group 4. Most of the proteins in group 1 were annotated as tRNA specific adenosine deaminases by NCBI (green), and some proteins were also annotated as cytidine and deoxycytidylate deaminases (pink). The protein under study, NE0047 (PDB entry 2G84), falls in group 5.

space group $P2_12_12_1$. The structure solution and further refinement were performed in CNS[30] using the native protein (PDB entry 2G84) as a search model for molecular replacement. Model building was conducted using COOT.[31] All figures were made using PyMOL.[32] Data collection and refinement statistics are summarized in Table 2.

Ligand Binding Experiments. Calorimetry was performed for NE0047 (full length and ΔC form of NE0047) with 8-azaguanine using MicroCal iTC200 (GE Healthcare). Samples were prepared in buffer containing 50 mM HEPES and 100 mM NaCl (pH 7.5) (buffer A). 8-Azaguanine (1.5 μL, 1.2 mM) was added with the syringe to the sample cell containing 25 μM full-length NE0047 or the ΔC mutant of NE0047 at a constant stirring rate of 1000 rpm. A total of 19 injections were performed for each experiment with an interval of 180 s between each successive injection. The temperature was maintained at 25 °C for all the ITC experiments. To nullify the heat of dilution, 8-azaguanine was titrated against buffer A and subtracted from the raw data prior to model fitting.

RESULTS

Computational Prediction of Enzyme Function. To predict the function of NE0047, the available sequences from cog0590 to which it belongs were used to construct a sequence similarity network, and Cytoscape was used for visualization[33] (Figure 1). Groups 1−3 are well-characterized and consist of tRNA specific adenosine deaminases (tRNA AD), GDs, and cytosine deaminases (CD), respectively. In the case of group 4, not much functional information is available; however, recent studies by Elias and Huang have shown that this group may contain RNA binding proteins.[34] Groups 5−8 consist of proteins of unknown function, annotated as putative dCMP/CMP deaminases. NE0047, the enzyme under study, falls in group 5. To extract the maximal possible amount of information from sequence alone, the sequence similarity network was constructed at both higher and lower cutoffs. However, an attempt to lower the blast cutoff resulted in coalescence of functionally unique clusters, putting many of the enzymes catalyzing different nucleobase deaminases in the same group. Conversely, a stringent cutoff resulted in redundant separation of functionally similar units into smaller groups.

In addition to sequence, because structural information was available for NE0047, a distance alignment (DALI) search was performed to find proteins that were structurally similar. DALI results against the query protein revealed that the top hits were tRNA AD (PDB entry 1Z3A), cytidine and deoxycytidylate deaminase (PDB entry 2A8N), *Bacillus subtilis* GD (*b*GD) (PDB entry 1WKQ), and yeast CD (yCD) (PDB entry 1UAQ) with the DALI *Z* scores being 19.7, 18.0, 17.9, and 17.2, respectively, and the root-mean-square deviations for C_α atoms for each of the deaminases being 2.0, 2.1, 1.9, and 2.7 Å performed using 145, 133, 155, and 151 residues, respectively. Apart from these hits, the riboflavin biosynthesis pathway enzymes were also observed in the list. A comparison of NE0047 with the top DALI hits also revealed that although these sequences exhibit a low level of sequence similarity, the overall fold was similar. In addition, each of these deaminases possesses structural elements that were unique to each protein. Analysis of the active site region of NE0047 with the top hits illustrates that the zinc binding region was identical in all these enzymes. In contrast, the ligand binding region showed a high degree of sequence and structural divergence and was not conserved among the various deaminases. Both the sequence

dx.doi.org/10.1021/bi400068g | *Biochemistry* 2013, 52, 3512−3522

and structural similarity studies suggest that NE0047 was a base deaminase. However, because of divergence in topological elements near the active site and a low level of sequence similarity (~30%), it became difficult to predict its exact function.

To establish the identity of the nucleobase that NE0047 deaminates and to filter out the potential nucleobase substrates of NE0047, docking studies using AutoDock version 4.2[26] were performed with a subset of compounds known to be involved in deamination reactions. Docking analysis revealed that purine and pyrimidine bases were easily accommodated in the NE0047 active site, whereas the corresponding nucleosides, although sometimes exhibiting high docking scores, failed to adopt geometry suitable for deamination. Additionally, it was found that the active site was too compact to accommodate the larger nucleotide moieties. Nucleotides like adenine, guanine, and cytidine di- and triphosphate therefore exhibit very low docking scores. Hence, docking studies implicated that the larger nucleotides were unlikely to be potential substrates of NE0047.

Experimental Validation. An independent experimental validation that NE0047 was indeed a nucleobase deminase was achieved by performing enzymatic deamination reactions with a series of purine and pyrimidine bases and their analogues using the Berthelot reaction (Figure S1 of the Supporting Information). By using nucleobase analogues, NE0047 was found to be catalytically active selectively toward guanine, and this reaction results in guanine undergoing a C2 deamination. Furthermore, to investigate the selectivity of NE0047 toward guanine, we also analyzed various guanine analogues for activity. The only nucleobase analogues that exhibited appreciable deamination potential as substrates of NE0047 were 8-azaguanine, ammeline, and 6-thioguanine (Scheme 1). Functionalization of the guanine base was not tolerated by NE0047 and resulted in a complete loss of activity.

Scheme 1. Structures of Ligands Shown To Be the Substrates for NE0047, (1) Guanine, (2) 8-Azaguanine, (3) Ammeline, and (4) 6-Thioguanine

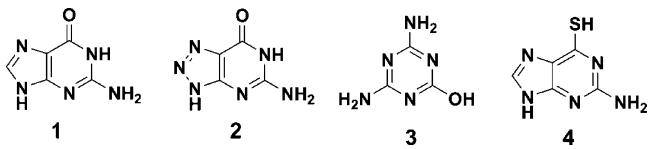

With the results obtained from the broad spectrum activity assay in hand, to assert and accurately analyze these findings, we conducted Michaelis–Menten kinetic studies on this enzyme with the potential substrates (Table 1). These results show that with guanine as a substrate, the catalytic efficiency of NE0047 is 1.2×10^5 M^{-1} s^{-1}. Comparison of the catalytic efficiency with values reported in literature reveals that it had activity comparable to those of other deaminases, which generally fall in the range of 10^4–10^6 M^{-1} s^{-1}. This value was an order of magnitude higher than that of human guanine deaminase, with a reported k_{cat}/K_m of 11.8×10^3 M^{-1} s^{-1}.[35] Kinetic studies of NE0047 with 8-azaguanine showed 70% activity as compared to that of guanine. However, in the case of 6-thioguanine, there was a drastic reduction in catalytic efficiency. Thus, the replacement of the oxygen atom at position 6 of the guanine ring with a sulfur atom, which also belongs to group VI in the periodic table and has electronic properties similar to those of oxygen, is not tolerated by the enzyme. Surprisingly, although the structure of ammeline is more divergent than those of other purine analogues that have been tested, NE0047 showed appreciable activity with ammeline and the catalytic efficiency was around 50% of that of guanine.

Table 1. Kinetic Parameters for Different Substrates of NE0047 at pH 7.0 and 37 °C

substrate	K_m (mM)	k_{cat} (s^{-1})	k_{cat}/K_m (M^{-1} s^{-1})
guanine	0.12 ± 0.01	15 ± 3	$(1.2 \pm 0.3) \times 10^5$
8-azaguanine	0.7 ± 0.03	6 ± 1	$(8.5 \pm 0.1) \times 10^3$
ammeline	1.8 ± 0.05	2 ± 1	$(1.1 \pm 0.5) \times 10^3$
6-thioguanine	–	–	$(2.1 \pm 0.5) \times 10^2$

Overall Structure of NE0047. To obtain a structural perspective of the interactions involved in deamination and the role played by the ligand binding site in fine-tuning specificity for a particular substrate, the crystal structures of native NE0047 and the catalytically dead form of the enzyme were determined in the presence of 8-azaguanine. The data processing and structural refinement statistics are listed in Table 2.

Table 2. Data Processing and Refinement Statistics

	NE0047–8-azaguanine (PDB entry 4HRQ)	NE0047 (E79A)–8-azaguanine (PDB entry 4HRW)
	Data Collection[a]	
resolution (Å)	1.9	2.43
wavelength (Å)	0.97	1.547
space group	$P2_12_12_1$	$P2_12_12_1$
no. of reflections	137052	77498
no. of unique reflections	25033	12160
redundancy	5.5 (5.1)	6.4 (6.1)
completeness	98.4 (95.9)	99.6 (98.1)
R_{sym} (%)	5.7 (29.2)	7.5 (24.7)
I/σ	18.4 (4.7)	15.7 (6.1)
	Refinement	
resolution (Å)	50–1.9	60–2.4
total no. of non-hydrogen atoms	2807	2720
no. of protein atoms	2785	2709
no. of ligand atoms	22	11
no. of water atoms	157	76
no. of reflections in refinement	22256	20240
no. of reflections in test set	2445	2109
R factor (%)	21.93	20.47
R_{free} (%)	24.48	26.47
root-mean-square deviation from ideal geometry		
bonds (Å)	0.0057	0.0059
angles (deg)	1.32	1.19
average B factor (Å^2)	52	38.07
Ramachandran plot (%)		
most favored region	96.5	95.1
additional allowed region	3.2	4.4
disallowed region	0.3	0.5

[a]Values for the highest-resolution shell are given in parentheses.

dx.doi.org/10.1021/bi400068g | Biochemistry 2013, 52, 3512–3522

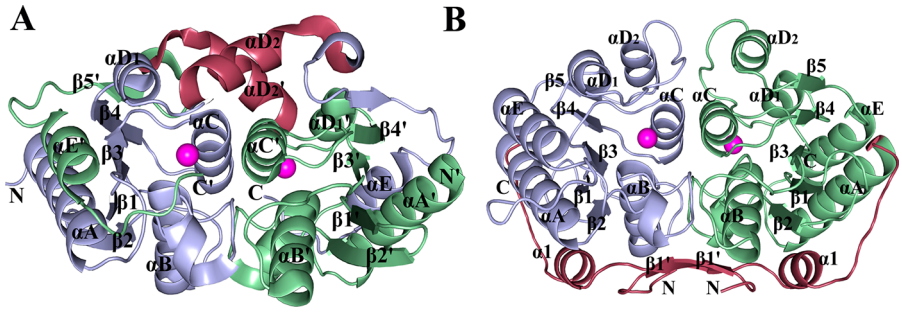

Figure 2. Cartoon representation of dimers of the two structurally characterized GDs: (A) *b*GD (PDB entry 1WKQ) and (B) NE0047. In both deaminases, subunit A is colored blue and subunit B green. Extra dimerization elements present in both deaminases are colored raspberry. Zinc is colored magenta.

The structure of NE0047 consists of a central five-stranded β sheet that is sandwiched by α helices αA, αE, and αD_1 on one side and αB, αC, and αD_2 on the other (Figure 2A). The β strand order is 2, 1, 3, 4, and 5, and β1 runs antiparallel to the other strands. This core fold is present in all CDA superfamily members, and the topology numbering system used here is identical to that of the previously reported structures of yCD[36] and *b*GD.[1] Along with these structural elements, NE0047 has extra elements that are unique to it and are labeled as α1 and $\beta 1'$ (helix−strand) in the N-terminal region (Figure 2B). Apart from the dimerization interface of NE0047, which is similar to those of other CDA superfamily members and is formed by packing of helices, αB and αC, these exclusive N-terminal elements form an extended dimerization interface that further intertwines the two subunits together. This results in NE0047 possessing a total dimeric buried surface area of 3755 Å^2 as compared to 3900 Å^2 in *b*Gd[1] and 1450 Å^2 in yCD.[36] Hence, it is evident that both *b*GD and NE0047 possess a more extensive dimeric interface, asserting the added importance of dimerization in the proper functioning of these enzymes (Figure 2).

Conformational Changes Associated with Ligand Binding. The electron density maps for both the native and mutant forms of NE0047 contained electron density for the ligand in the active site (Figure 3B). Compared to that of the apo form of the enzyme, binding of the ligand did not cause major conformational changes in subunit A of the protein, where the loop is exposed to the solvent and residues Cys180 and Cys189 form a disulfide bond (Figure S2 of the Supporting Information). However, in subunit B, a nine-amino acid loop at the extreme C-terminus (residues 180−189), which was disordered in the apo form of the enzyme, became ordered upon ligand binding (Figure 3A). The density for this loop was noisy, and only the backbone peptide bonds could be fit. Side chain density was not clearly visible; therefore, a polyalanine model was fit (Figure S3 of the Supporting Information). For this nine-residue loop region in subunit B, the *B* factor values are in the range of 40−70 Å^2. Comparison of the extreme C-terminal nine-amino acid loop region of the two subunits of NE0047 shows that this loop region exhibits a major conformational change, and the subunit B loop moves into the active site cavity by a distance of 13 Å (Figure 3A). The structural data strongly indicate that conformational changes in this loop play a major role in catalysis, especially in protecting the active site from the surrounding solvent and in limiting the size of the ligand. The presence of a disulfide bond in the open conformation is a coincidental finding in NE0047 and not essential for enzyme activity, as disruption of the disulfide bridge via the C180S mutation does not cause any loss of activity. Positions C180 and C189 are also not conserved across the group 5 enzymes.

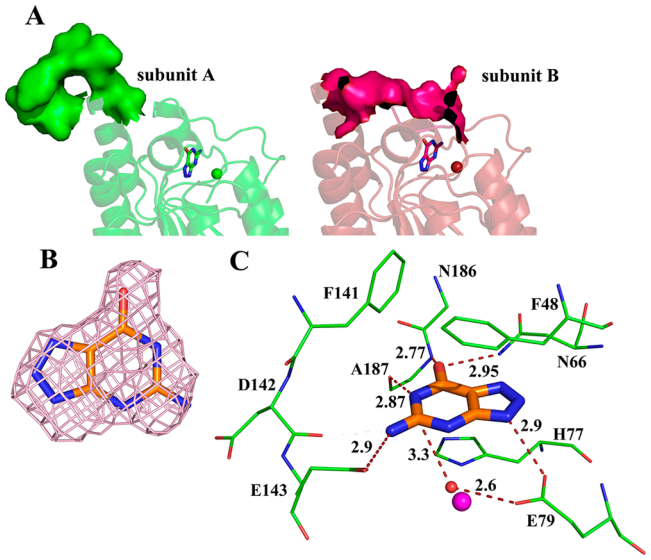

Figure 3. Conformational change upon ligand binding and active site architecture. (A) Cartoon representation of the open and closed forms of the enzyme depicting the conformational change observed in subunit B. The C-terminal loop is shown as a surface representation; the zinc atom and the carbon atoms of the bound ligand are colored green in subunit A and pink in subunit B. (B) Electron density ($F_o - F_c$) map contoured at 3.5σ for 8-azaguanine. (C) Interaction network of 8-azaguanine in the subunit B active site of NE0047. Carbon atoms of the ligand are colored orange and those of the ligand binding residues green. The Zn atom is colored magenta and the catalytic water red. Oxygen atoms are colored red and nitrogen atoms blue.

Active Site Architecture. The geometry of the zinc atom is tetrahedral and is coordinated by Cys112 (2.4 Å), Cys115 (2.4 Å), His77 (2.1 Å), and a water molecule (2.3 Å) (Figure S4 of the Supporting Information). In subunit A of NE0047, 8-azaguanine is bound in the active site cleft formed by the zinc binding region on one side and capped by the loop spanning residues 140−145 between helix αD_1 and αD_2 on the other. This loop region consists of a phenylalanine residue, an aspartatic acid residue, and a glutamic acid residue, which are involved in the correct positioning of the substrate into the active site and may play a major role in assisting deamination. Moreover, as shown in Figure 3C, the purine ring of the ligand is stabilized by hydrophobic interactions of the benzene ring of Phe141 present on this loop. Further stabilization of the purine ring is achieved by additional hydrophobic interactions with

dx.doi.org/10.1021/bi400068g | *Biochemistry* 2013, 52, 3512−3522

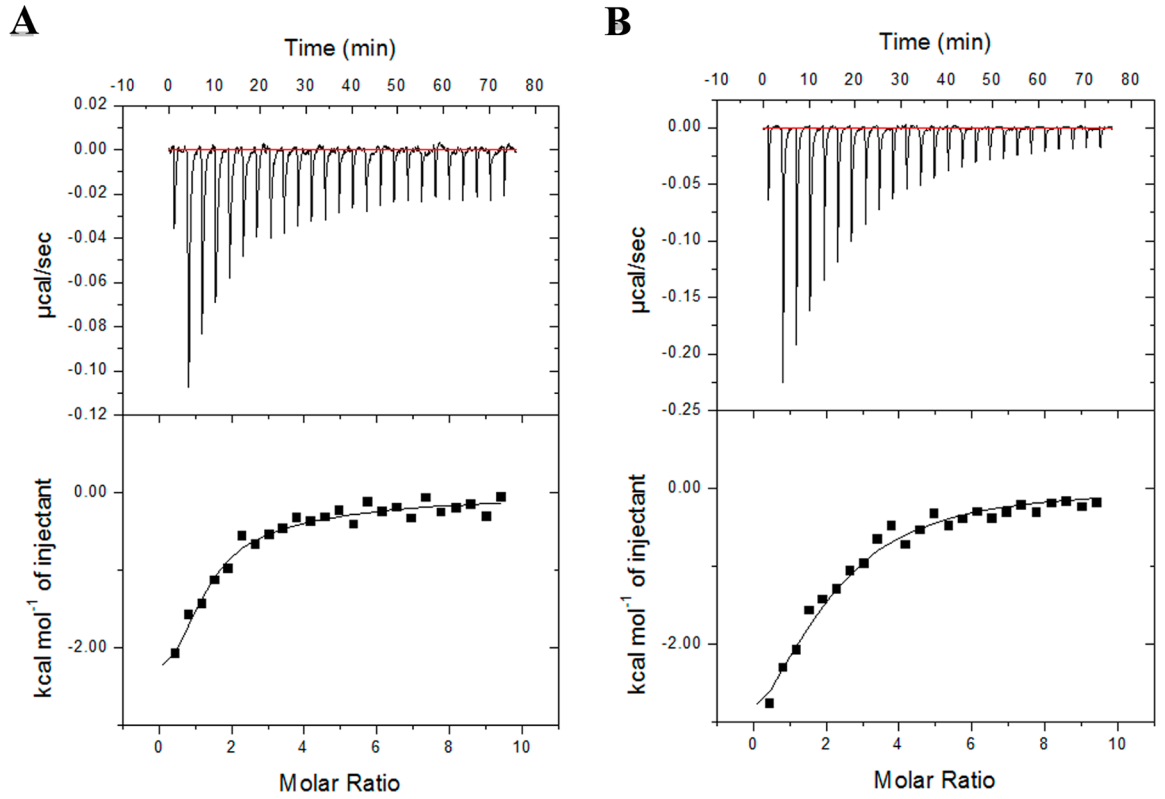

Figure 4. Differential mode of ligand binding in NE0047 variants. (A) ITC data for titration of 8-azaguanine into full-length NE0047 in 50 mM HEPES and 100 mM NaCl buffer. The solid line in the bottom panel represents the best fit using the sequential binding model with a $K_{1,ITC}$ of (1.4 ± 0.37) × 10^5 M^{-1} and a $K_{2,ITC}$ of (6.1 ± 0.9) × 10^3 M^{-1}. (B) ITC data for titration of 8-azaguanine into the ΔC form of NE0047 in 50 mM HEPES and 100 mM NaCl buffer. The solid line represents the best fit using a one set of sites binding model with an n_{ITC} of 1.92 and a K_{ITC} of (3.2 ± 0.3) × 10^4 M^{-1}.

Phe48 lying on helix αC and the metal binding histidine residue His77. In the ligand binding pocket, the amino group of 8-azaguanine is positioned close to the zinc binding region and is anchored in position by hydrogen bonding interactions with $O^{\varepsilon 1}$ of Glu143 (2.9 Å). The zinc-bound catalytic water molecule is 3.3 Å from the C2 atom of guanine and positioned optimally for subsequent nucleophilic attack. Apart from this, the O6 atom of the purine ring of 8-azaguanine forms a hydrogen bonding interaction with the $N^{\delta 2}$ atom of the Asn66 residue within a distance of 2.9 Å. In subunit B, almost all the interactions of 8-azaguanine are conserved; however, because of the closing of the C-terminal flap, this region also contributes to the stabilization of the ligand. The O6 atom of 8-azaguanine makes additional hydrogen bonds with the backbone nitrogen atom of Ala187 with a distance of 2.8 Å, and the N1 atom of 8-azaguanine is 2.9 Å from the carbonyl oxygen of Ala187 (Figure 3C).

Effect of Deletion of the C-Terminal Loop. Isothermal titration calorimetry (ITC) was used as a primary technique to understand the mode of substrate binding. The thermodynamic parameters of the generation of ligand−protein complexes were determined (Figure 4), with the heat profiles depicting a complex formation by an exothermic mode of 8-azaguanine binding. The ΔH and ΔS values for the full-length native version of the enzyme are as follows: ΔH_1 = −2.88 ± 0.2 kcal/mol, ΔH_2 = −4.05 ± 7.5 kcal/mol, ΔS_1 = 13.9 cal mol^{-1} deg^{-1}, and ΔS_2 = 1.65 cal mol^{-1} deg^{-1}. For the ΔC version of the enzyme, which has the extreme nine amino acids deleted and hence does not contain the conformationally flexible C-terminal loop region, ΔH = −4.6 ± 0.1 kcal/mol and ΔS = 5.08 cal mol^{-1} deg^{-1}. The values of ΔH suggest that the interactions between the ligand and protein were highly enthalpy-driven. This may be due to the energy released upon binding of the ligand to the active site. The heat profile for the full-length dimeric form of the enzyme fits well to a sequential binding mode, which helps us to conclude that the binding of the ligand to the dual active site system follows an allosteric communication model. Attempts to fit this heat profile in a one set of sites model failed. However, the deletion mutant (ΔC) results in the enzyme following an independent binding site model exhibiting no communication between active sites. Moreover, the deletion of the loop did not result in an appreciable change in the binding affinity of 8-azaguanine. These observations lead to the conclusion that although the ligand can still bind to the individual active site cavities, it no longer exhibits interdomain communication. Additional, activity assays of the deletion mutant (ΔC) showed that removal of the extreme nine amino acid residues results in a complete loss of activity (Figure S1B of the Supporting Information).

DISCUSSION

Identification of the Function of NE0047. NE0047 was found to be primarily a purine deaminating enzyme that in particular catalyzes the hydrolytic deamination of guanine to xanthine in a proficient fashion and also exhibited secondary activity toward ammeline (Scheme 2). Assigning the function of NE0047 as a GD using sequence alone was nontrivial mostly because it exhibits sequence divergence with known GDs. Hence, an exhaustive sequence similarity search using all

dx.doi.org/10.1021/bi400068g | Biochemistry 2013, 52, 3512−3522

Scheme 2. Deamination Reactions Catalyzed by NE0047

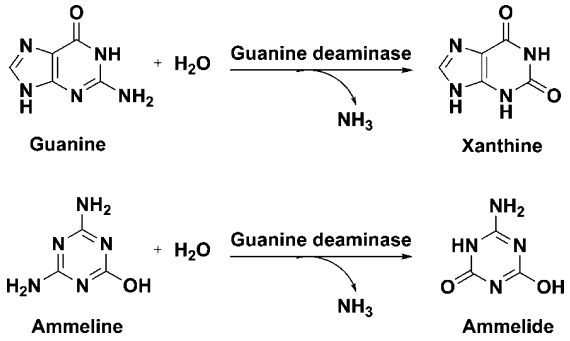

members of the cog0590 to which NE0047 belongs failed to catalogue NE0047 in the group of enzymes annotated as GDs (Figure 1). Moreover, NE0047 also exhibits structural divergence, and therefore, using structure as a guide to function was inconclusive in annotation of the exact function of the protein. However, both sequence and structural information were successful in narrowing the function of NE0047 as a plausible nucleobase deaminating enzyme. Comparison of the structure of NE0047 with *b*GD, which is a representative member of the known GDs, helped us to understand why structural similarity alone failed to annotate NE0047 as a GD (Figure 2). The active site elements that form the binding pocket differ between the enzymes. *b*GD has a domain-swapped structure with the active site composed of elements from both subunits. Helix αD_2 from each subunit crosses over, so that the C-terminal end of each subunit intertwines with the neighboring subunit[1] (Figure 2A). On the other hand, unlike *b*GD, in NE0047 the active site is entirely within a single monomer. Helix αD_2 in this case is shorter and does not directly participate in stabilization of the ligand. Instead, in NE0047 the region between helices αD_1 and αD_2 is replaced by a 10-amino acid loop that contains catalytically important residues that, although they show a high degree of similarity, are not identical between the two GDs.

For deciphering the function of NE0047, using structure as a guide to function was additionally difficult as the two structures available for comparison were the imidazole-bound form of *b*GD and the apo form of NE0047, both of which showed considerable variation in the ligand binding region. The reported structure of the imidazole-bound form of *b*GD exhibited an intersubunit interaction of the C-terminal tail, where the extreme C-terminal residue was found to be a conserved tyrosine that interacts with the bound ligand.[1] However, the structure of the apo form of NE0047 deposited as part of the structural genomics effort not only showed no intersubunit interaction but also had the C-terminal tail oriented approximately 15 Å from the active site. Moreover, the C-terminally conserved tyrosine residue present in all reported CDA superfamily GDs (belonging to group 2) was also missing and was instead replaced by a cysteine residue. This cysteine residue, at position 189, was found to form a disulfide bond with the cystine residue at position 180; thus, in contrast to the case for *b*GD, this resulted in the C-terminal loop being exposed to the solvent.

Apart from the variation in the C-terminal region, the N-terminal region of both the GDs also varies. A further analysis of the structure of *b*GD and NE0047 showed that they both require an extensive dimerization interface, which is almost double the size of that of other CDA superfamily members. The excess interactions are achieved in a different fashion in both the enzymes. *b*GD uses the domain swapping helix αD_2 for dimerization, whereas NE0047 utilizes the additional unique strand−helix motif at the N-terminal region that interdigitates and seals the dimerization interface (Figure 2B). Thus, it can be concluded that because of the evolutionary divergence exhibited between *b*GD and NE0047, the strategy of using structure as a guide to function failed. In addition, we also conclude that enzymes that fall in group 5 in the sequence similarity network (Figure 1) are also GDs and cluster as a separate group because of divergent evolution. Therefore, it is highly possible that other groups (Figure 1) with unknown function in the sequence similarity network may also possess functions similar to those of members of groups 1−4. However, they appear in separate groups because of evolutionary divergence.

The secondary activity of NE0047 toward ammeline was another surprising discovery. Our activity assay studies show that NE0047 is not a promiscuous enzyme by nature. The results clearly show that NE0047 does not show any activity toward the other most common nucleobase or their nucleoside and nucleotide analogues. Therefore, the deamination of ammeline by NE0047 is not coincidental but has some physiological importance. A literature search of the known GDs showed that GDs from the AHS (from *Bradyrhizobium japonicum*) have previously been reported to catalyze the deamination of ammeline.[37] These GDs deaminate ammeline as their secondary activity, and the reports demonstrated that most organisms do not possess unique enzymes to deaminate ammeline but rather employ the endogenous GDs for this reaction.[37] NE0047 is the first report of a GD from the CDA superfamily that exhibits a moonlighting activity toward ammeline. Ammeline is a substituted triazine intermediate produced in the bacterial metabolism of melamine, a chemical adulterant found in pet foods and infant formula that causes mortality in pets and children.[38] Bacteria metabolize melamine via three consecutive deamination reactions to generate cyanuric acid or uric acid.[39] In the second deamination reaction, ammeline is the substrate. These findings stress the fact that even when the function of an enzyme is obvious using both structure and sequence, it may become necessary to use experimental validation methods, especially in cases where a protein may catalyze multiple reactions with varying degrees of substrate specificity.

Structural Basis of Substrate Specificity. The X-ray structure of NE0047 with 8-azaguanine was valuable in understanding the structural basis of ligand specificity. The crystal structure reveals that NE0047 has evolved to engineer an active site that has the purine base placed in the active site crevice, close to the catalytic zinc. NE0047 exhibits extreme sensitivity toward functional tweaking of the purine ring; even a slight alteration of the heterocyclic ring drastically affects catalytic activity. For example, activity assay results show that 1-methylguanine exhibits no deamination. This can be explained by using the crystal structure orientation of 8-azaguanine as a starting orientation and then theoretically building further functional groups on it. An addition of a methyl group at the N1 position of the base to the existing orientation as observed in the X-ray structure will result in a steric clash with the hydrophobic Phe141 residue capping the active site, thus forcing the molecule to rearrange in the active site and adopt a conformation that is catalytically nonproductive. Similarly, substitution of a bulky sulfur atom in place of an oxygen atom

dx.doi.org/10.1021/bi400068g | *Biochemistry* 2013, 52, 3512−3522

Scheme 3. Proposed Mechanism of Deamination by NE0047

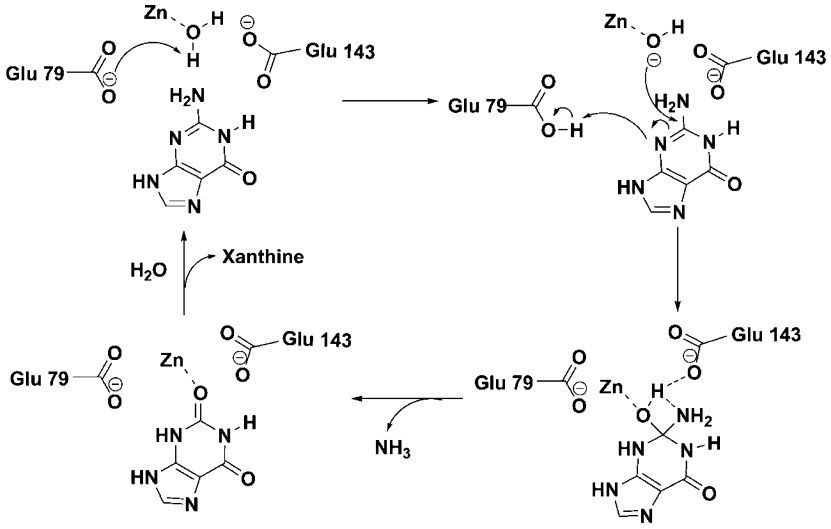

at position 6 of the base significantly reduces enzyme activity because it most probably interferes with the correct positioning of Asn66, leading to inappropriate anchoring of the purine base. Even the alternate purine base, adenine, is not accepted as a substrate, mostly because if it occupies a conformation similar to that of guanine, the amino group attached to the C6 atom of adenine faces away from the zinc site toward Asn66, in a catalytically unfavorable conformation. Further, to understand why guanylic derivatives like guanosine and dGMP are not accepted as substrates, an attempt to extend the structure by fixing the guanine ring in the crystallographic position was undertaken. Introduction of either the sugar or the sugar–phosphate moiety into the apo form of the enzyme results in a steric clash with the backbone of the enzyme; thus, it is evident that the active site is too compact to accommodate the larger nucleoside and nucleotide analogues. These findings reflect the importance of the fidelity of guanine deamination in biology.

Apart from guanine, ammeline was the only other competent substrate deaminated by NE0047. Ammeline is structurally similar to cytosine; therefore, the fact that NE0047 is unable to deaminate cytosine was unforeseen. It is highly likely that both electronic and size factors are involved in discrimination of cytosine versus ammeline by NE0047. The small size of cytosine most probably impedes a proper anchoring of the compound into the GD active site. However, in the case of ammeline, the presence of an extra nitrogen atom in the heterocyclic ring and a substitution of a diamino group are probably adequate to satisfy both electronic factors and scaffold design required by NE0047 to deaminate it.

Role of the C-Terminal Loop in Controlling Catalytic Activity. To avoid functional promiscuity and to ensure proper anchoring of the smaller bases like cytosine and guanine, we found that in most of the base deaminases, steric requirements are made stringent by addition of extra C-terminal topological elements. This regulation is missing in the large substrate accommodating nucleoside and nucleotide deaminating enzymes. In NE0047, we were able to crystallographically trap both the open and closed forms of the enzyme. Comparison of the X-ray structure of the apo form of NE0047 with that of 8-azaguanine revealed that ligand binding induces a closure of the solvent-exposed loop in subunit B of the enzyme (Figure 3A and Figure S3 of the Supporting Information). In subunit A, this loop region is in the open form with the residues being ordered and exposed to the solvent, whereas in subunit B, this loop closes like a flap on top of the ligand and also participates in stabilization of the guanine moiety. Therefore, we believe that we have trapped the enzyme in two different states along the reaction coordinate. The purpose of the loop is twofold: (1) limiting the size of the substrate and (2) creating a favorable environment for deamination to proceed efficiently. As mentioned earlier, the C-terminal region of *b*GD is also involved in ligand stabilization and utilizes a conserved tyrosine residue that is absent in NE0047. However, unlike *b*GD, because NE0047 does not have a C-terminal tyrosine residue, it achieves ligand stabilization by utilizing the peptide backbone for the same purpose, thus eliminating the need for sequence conservation among group 5 GDs.

The importance of this loop region in NE0047 was further investigated using activity assay and calorimetric studies. Activity assay studies of the C-terminal loop deletion mutant that has the extreme nine amino acids missing show that the ΔC form of the enzyme is catalytically incompetent, proving that this region is extremely important for enzyme activity (Figure S1B of the Supporting Information). This observation is not an outcome of instability introduced into the secondary structure by deletion of this region as circular dichroism studies show that both the full-length form and the ΔC form fold properly. Additional ITC data demonstrate that the full-length enzyme exhibits a sequential order of ligand binding, where binding of ligand to one monomer is communicated to the second active site and thus the system follows a cooperative allosteric model of ligand occupancy, whereas the ΔC form of the enzyme follows an independent site binding model (Figure 4). It was also observed that the binding affinity of the 8-azaguanine molecule is not significantly affected by deletion of the C-terminal loop; hence, only the interdomain communication is destroyed, and though the molecule is rendered catalytically incompetent, it is still able to retain binding of the ligand. Analysis of the crystal structure shows that the most probable mode of communication between the two subunits is via the dimeric interface. The binding of the guanine base induces a conformational change and results in closure of the C-terminal flap. As observed in the structure, the closure of the

dx.doi.org/10.1021/bi400068g | *Biochemistry* 2013, 52, 3512–3522

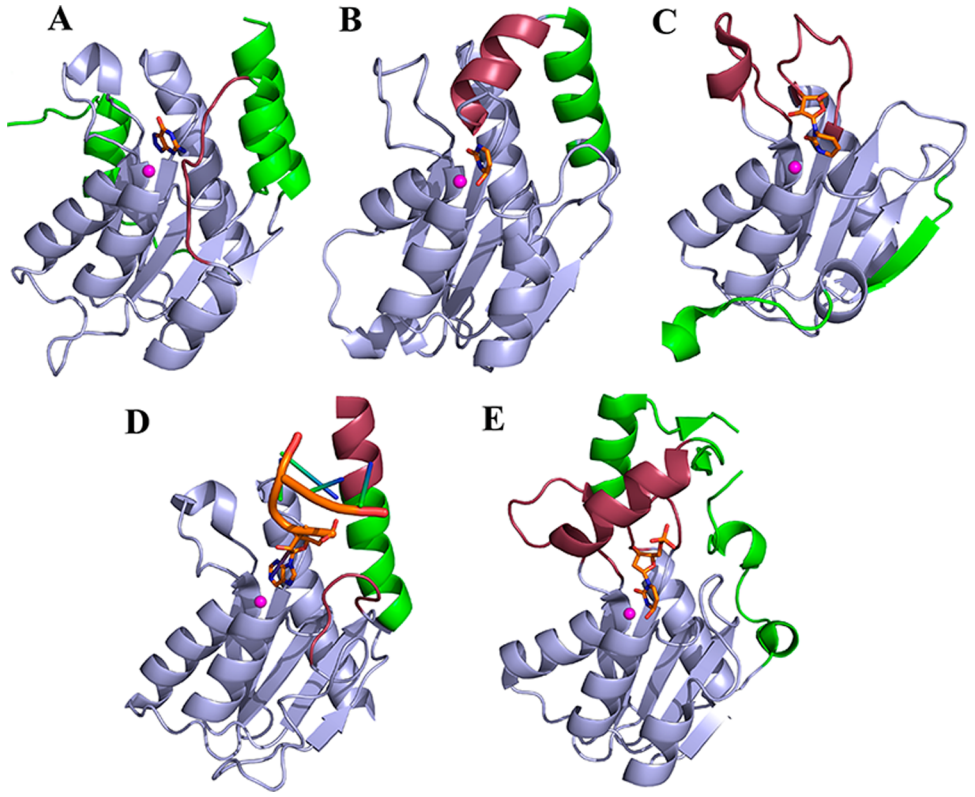

Figure 5. Evolution of the deaminase fold of the CDA superfamily: (A) NE0047, (B) yeast cytosine deaminase, (C) human cytidine deaminase (PDB entry 1MQ0), (D) tRNA specific adenosine deaminase, and (E) T4 bacteriophage deoxycytidylate deaminase (PDB entry 1VQ2). In all deaminases, common CDA superfamily fold elements are colored light blue. The catalytically important regions unique to each protein are colored raspberry. Other additional elements are colored green. In all structures, the carbon atoms of the bound ligands are colored orange and the zinc atom is colored magenta. Oxygen atoms are colored red and nitrogen atoms blue.

C-terminal flap region in subunit B of the protein brings this region into the proximity of the 10-amino acid catalytic loop lying between regions αD_1 and αD_2, spanning residues 140–149. While the C-terminal part of this catalytic loop is involved in interactions with the ligand and modulates catalysis, the N-terminal part is involved in formation of the dimerization interface. Therefore, the closure of the C-terminal flap can induce the catalytic loop to communicate the advance of the reaction to the other subunit by transferring the signal efficiently via the dimeric interface. These observations lead us to conclude that the closed form as seen in subunit B is the catalytically active form of the enzyme and the open conformation is the state involved in product release. This is the first study in which this mode of extended catalytic communication has been investigated in any deaminases belonging to the AHS or CDA superfamily reported to date. Thus, the results show that the C-terminal region not only is required for enzyme activity but also plays a pivotal role in interdomain crosstalk, and it is the overall conformation adopted by the C-terminal region and not the specific sequence that confers activity to the group 5 GDs.

Molecular Mechanism of Deamination. Utilizing the information from the crystal structure of the 8-azaguanine-bound enzyme and literature available on zinc-assisted deaminases, a mechanism of deamination of guanine by NE0047 has been proposed (Scheme 3). It is apparent from the crystal structure that the correct positioning of the amino group of guanine is paramount for conferring activity. All deaminases contain a catalytically conserved glutamic acid residue (Glu79 in NE0047), which is proposed to be involved in catalysis and serves as a proton transporter.[1,36] Abstraction of the proton from the zinc-bound water results in the formation of the nucleophilic hydroxide ion, which subsequently attacks the C2 atom of guanine adjacent to the amino group to be deaminated. We suggest that the stabilization of the transition state is further achieved by the shuttling of the same proton to the N3 atom of guanine. Apart from Glu79, NE0047 also contains a Glu143 in the vicinity of the substrate, and we propose that it plays a pivotal role in deamination. Structural comparison of NE0047 with *b*GD shows that this residue is replaced by an equivalent negatively charged aspartic acid residue in *b*GD (Asp114). Hence, our findings confirm that this residue also plays a similar role in *b*GD. Therefore, we propose, while Glu79 is responsible for stabilization of the transition state, Glu143 is involved in facilitating collapse of the tetrahedral intermediate (Scheme 3). Glu143, like Glu79, also acts as a proton transporter and abstracts the proton from the activated hydroxide, which bridges the zinc ion with the C2 atom of guanine and delivers it to the amino group of guanine, resulting in the release of ammonia. Mutation of both these key catalytic residues, Glu79 and Glu143, present in NE0047 to alanine results in a complete loss of activity (Figure S1B of the Supporting Information).

Previous computational mechanistic studies performed on the *b*GD system attempted to use the crystallographic position of the imidazole moiety to decipher the fine details of the mechanism.[40] A superposition of the imidazole-bound *b*GD onto the azaguanine-bound NE0047 structure reveals that the imidazole ring occupies a position closer to the six-membered part of the fused heterocycle as opposed to the previous overlay

dx.doi.org/10.1021/bi400068g | *Biochemistry* 2013, 52, 3512–3522

onto the five-membered ring used for the computational mechanistic study.[40] This resulted in a model in which Asp114 (analogous to Glu143 in NE0047) interacted with the N9 atom as opposed to the amino group adjacent to the C2 atom as seen in the crystal structure. Thus, the availability of a more precise positioning of guanine from the crystal structure will aid in a future more accurate study. Structural comparison of the guanine deaminases with cytosine/cytidylic deaminases reveals that in the latter case only a single glutamic acid-based proton shuttling mechanism is observed.[41,42] This may be caused by the smaller size of the pyrimidine ring, where the same glutamic acid residue can both abstract and donate the proton. However, the larger purine base ADs have been suggested to utilize a combination of glutamic acid and histidine pairs to effectively catalyze the deamination reaction.[42]

Evolution of the CDA Superfamily. The CDA superfamily members present an elegant example of evolution of enzyme structure to facilitate enzyme function. An analysis of the ligand-bound X-ray structures of the available CDA superfamily members, yCD,[36] human cytidine deaminase (hCD),[43] dCMP,[44] and tRNA AD,[3] with NE0047 reveals that although the core fold is conserved, the region around the active site is modulated to render substrate specificity (Figure 5). While the nucleoside and nucleotide accepting deaminases have a more open active site, the base deaminases like GDs and CDs have devised structural elements to allow compaction of the active site. For example, both GDs and CDs contain extra C-terminal regions that limit the size of the active site pocket and are also involved in conferring substrate specificity by preventing the entry of the larger nucleoside and nucleotide scaffolds. This C-terminal region is well-defined in the form of an extra helix, αF, like in yCD,[36] or can be mobile as observed in NE0047. The nucleotide and nucleoside deaminating deaminases lack the C-terminal topological elements and have evolved to accommodate unique loop insertions present between αA and β1 and between β2 and αB in the CDA superfamily fold to facilitate the binding of the ribose sugar moiety.[43,44] This loop region consists of a conserved glutamic acid (Glu56 in hCD) that forms a hydrogen bond with the 3′-OH group of the sugar moiety, hence allowing for its stabilization.[43] Furthermore, the nucleotide catalyzing deaminases like dCMP deaminases have evolved to introduce an insertion of an extra helix and a loop moiety that replaces helix αD_1 of NE0047. This helix consists of positively charged residues, for example, arginine residues that constitute a pocket for the stabilization of a negatively charged phosphate group.[44] On the other hand, the tRNA ADs have modified their fold to add an extra helix αE at the C-terminal end and in place of helix αD_1 of NE0047 have an insertion of a long loop region. Both of these unique elements in tRNA ADs make extensive interactions with the RNA moiety, conferring it specificity toward its substrate.[3]

A closer examination of the positioning of the base into the active site of each deaminase provided clues about the strategies adopted by nature to differentially assist particular deamination reactions. A comparison of the ligand-bound structures of pyrimidine base deaminating enzymes revealed all enzymes that assist a C4 deamination of the pyridyl nitrogen atom have the cytosine base positioned in a similar orientation. However, a comparison of the purine deaminating enzymes with the pyridimine deaminating enzymes reveals that although both bases bind in the vicinity of the zinc ion, the overall orientation is markedly different. Depending on the purine base to be deaminated, the active site interactions are modulated to position either the guanine or the adenine moiety in a catalytically favorable conformation. For example, in both NE0047 and tRNA AD, the purine base occupies roughly the same overall position; however, the orientation of the purine base is flipped by 180° in tRNA AD with respect to that in NE0047. This allows the enzymes to adopt an orientation so that a C2 deamination in the case of guanine and a C6 deamination in the case of adenosine can occur efficiently. Hence, in conclusion, a structural analysis of the CDA superfamily fold reveals that this fold has deftly evolved and restructured its active site by deleting or adding elements requisite for a particular substrate.

■ ASSOCIATED CONTENT

Ⓢ Supporting Information

Figures S1−S4. This material is available free of charge via the Internet at http://pubs.acs.org.

■ AUTHOR INFORMATION

Corresponding Author

*Department of Chemistry, IIT Bombay, Powai, Mumbai, India 400076. Telephone: 91-25767165. Fax: 91-25767152. E-mail: ruchi@chem.iitb.ac.in.

Present Address

†B.H.: IITB-Monash Research Academy, Old CSE Building, 2nd Floor, IIT Bombay, Powai, Mumbai 400076, India.

Author Contributions

The manuscript was written through contributions of all authors. All authors have given approval to the final version of the manuscript.

Author Contributions

‡B.H. and A.S.T. contributed equally to this work.

Funding

This work was supported by IIT Bombay, DBT (BT/PRI3766/BRB/10/785/2010) and DST (SR/S/BB-53/2010).

Notes

The authors declare no competing financial interest.

■ ACKNOWLEDGMENTS

We thank the Midwest Center for Structural Genomics Consortium for providing the NE0047 plasmid. We thank the DBT-India consortium and BM-14 at the European Synchrotron Radiation Facility (ESRF) and the National Institute of Immunology (Delhi, India) for providing the facilities for X-ray data collection. We also thank Ravi Joriga, a Masters student at IIT Bombay, for initial standardization of the ammonia assay.

■ ABBREVIATIONS

PDB, Protein Data Bank; CDA, cytidine deaminase; *b*GD, *B. subtilis* guanine deaminase; GD, guanine deaminase; CD, cytosine deaminase; yCD, yeast cytosine deaminase; tRNA AD, tRNA specific adenosine deaminase; hCD, human cytidine deaminase; AutoDock, automated docking tool; ITC, isothermal titration calorimetry; TEV, tobacco etch virus; ΔC, NE0047 (residues 1−180); AHS, amidohydrolase superfamily.

■ REFERENCES

(1) Liaw, S. H., Chang, Y. J., Lai, C. T., Chang, H. C., and Chang, G. G. (2004) Crystal Structure of *Bacillus subtilis* Guanine Deaminase. *J. Biol. Chem.* *279*, 35479−35485.

(2) Pang, B., McFaline, J. L., Burgis, N. E., Dong, M., Taghizadeh, K., Sullivan, M. R., Elmquist, C. E., Cunningham, R. P., and Dedon, P. C. (2012) Defects in purine nucleotide metabolism lead to substantial incorporation of xanthine and hypoxanthine into DNA and RNA. *Proc. Natl. Acad. Sci. U.S.A. 109*, 2319−2324.
(3) Losey, H. C., Ruthenburg, A. J., and Verdine, G. L. (2006) Crystal structure of *Staphylococcus aureus* tRNA adenosine deaminase TadA in complex with RNA. *Nat. Struct. Mol. Biol. 13*, 153−159.
(4) Berger, S. J., Carter, J. G., and Lowry, O. H. (1985) Distribution of guanine deaminases in mouse brain. *J. Neurochem. 44*, 1736−1740.
(5) Paletzki, R. F. (2002) Cloning and characterization of guanine deaminase from mouse and rat brain. *Neuroscience 109*, 15−26.
(6) Kuzmits, R., Seyfried, H., Wolf, A., and Müller, M. M. (1980) Evaluation of serum guanase in hepatic diseases. *Enzyme 25*, 148−152.
(7) Seibert, C. M., and Raushel, F. M. (2005) Structural and Catalytic Diversity within the Amidohydrolase Superfamily. *Biochemistry 44*, 6383−6391.
(8) Lai, W. L., Chou, L. Y., Ting, C. Y., Kirby, R., Tsai, Y. C., Wang, A. H. J., and Liaw, S. H. (2004) The Functional Role of the Binuclear Metal Center in D-Aminoacylase. *J. Biol. Chem. 279*, 13962−13967.
(9) Bateman, A., Birney, E., Cerruti, L., Durbin, R., Etwiller, L., Eddy, S. R., Griffiths-Jones, S., Howe, K. L., Marshall, M., and Sonnhammer, E. L. L. (2002) The Pfam Protein Families Database. *Nucleic Acids Res. 30*, 276−280.
(10) Reizer, J., Buskirk, S., Bairoch, A., Reizer, A., and Saier, M. H., Jr. (1994) A novel zinc-binding motif found in two ubiquitous deaminase families. *Protein Sci. 3*, 853−856.
(11) Hall, R. S., Fedorov, A. A., Xu, C., Fedorov, E. V., Almo, S. C., and Raushel, F. M. (2011) Three-Dimensional Structure and Catalytic Mechanism of Cytosine Deaminase. *Biochemistry 50*, 5077−5085.
(12) Hitchcock, D. S., Fedorov, A. A., Fedorov, E. V., Dangott, L. J., Almo, S. C., and Raushel, F. M. (2011) Rescue of the Orphan Enzyme Isoguanine Deaminase. *Biochemistry 50*, 5555−5557.
(13) Baker, D., and Sali, A. (2001) Protein structure prediction and structural genomics. *Science 294*, 93−96.
(14) UniProt Consortium (2009) The Universal Protein Resource (UniProt). *Nucleic Acids Res. 37*, D169−D174.
(15) Schneider, M., Tognolli, M., and Bairoch, A. (2004) The Swiss-Prot protein knowledgebase and ExPASy: Providing the plant community with high quality proteomic data and tools. *Plant Physiol. Biochem. 42*, 1013−1021.
(16) Schnoes, A. M., Brown, S. D., Dodevski, I., and Babbitt, P. C. (2009) Annotation error in public databases: Misannotation of molecular function in enzyme superfamilies. *PLoS Comput. Biol. 5*, e1000605.
(17) Gerlt, J. A., and Babbitt, P. C. (2000) Can sequence determine function? *Genome Biol. 1*, REVIEWS0005.
(18) Hermann, J. C., Marti-Arbona, R., Fedorov, A. A., Fedorov, E., Almo, S. C., Shoichet, B. K., and Raushel, F. M. (2007) Structure-based activity prediction for an enzyme of unknown function. *Nature 448*, 775−779.
(19) Dunbrack, R. L., Jr. (2006) Sequence comparison and protein structure prediction. *Curr. Opin. Struct. Biol. 16*, 374−384.
(20) Qu, X., Swanson, R., Day, R., and Tsai, J. (2009) A guide to template based structure prediction. *Curr. Protein Pept. Sci. 10*, 270−285.
(21) Pegg, S. C., Brown, S. D., Ojha, S., Seffernick, J., Meng, E. C., Morris, J. H., Chang, P. J., Huang, C. C., Ferrin, T. E., and Babbitt, P. C. (2006) Leveraging enzyme structure-function relationships for functional inference and experimental design: The structure-function linkage database. *Biochemistry 45*, 2545−2555.
(22) Gerlt, J. A. (2007) A Protein Structure (or Function?) Initiative. *Structure 15*, 1353−1356.
(23) Kim, S. H., Shin, D. H., Choi, I. G., Schulze-Gahmen, U., Chen, S., and Kim, R. (2003) Structure-based functional inference in structural genomics. *J. Struct. Funct. Genomics 4*, 129−135.
(24) Perona, J. J., and Craik, C. S. (1997) Evolutionary divergence of substrate specificity within the chymotrypsin-like serine protease fold. *J. Biol. Chem. 272*, 29987−29990.
(25) Gerlt, J. A., and Babbitt, P. C. (1998) Mechanistically diverse enzyme superfamilies: The importance of chemistry in the evolution of catalysis. *Curr. Opin. Chem. Biol. 2*, 607−612.
(26) Morris, G. M., Huey, R., Lindstrom, W., Sanner, M. F., Belew, R. K., Goodsell, D. S., and Olson, A. J. (2009) AutoDock4 and AutoDockTools4: Automated docking with selective receptor flexibility. *J. Comput. Chem. 30*, 2785−2791.
(27) Caraway, W. T. (1966) Colorimetric Determination of Serum Guanase Activity. *Clin. Chem. 12*, 187−193.
(28) Battye, T. G. G., Kontogiannis, L., Johnson, O., Powell, H. R., and Leslie, A. G. W. (2011) iMOSFLM: A new graphical interface for diffraction-image processing with MOSFLM. *Acta Crystallogr. D67*, 271−281.
(29) Evans, P. (2006) Scaling and assessment of data quality. *Acta Crystallogr. D62*, 72−82.
(30) Brunger, A. T., Adams, P. D., Clore, G. M., DeLano, W. L., Gros, P., Grosse-Kunstleve, R. W., Jiang, J. S., Kuszewski, J., Nilges, M., Pannu, N. S., Read, R. J., Rice, L. M., Simonson, T., and Warren, G. L. (1998) Crystallography & NMR system: A new software suite for macromolecular structure determination. *Acta Crystallogr. D54*, 905−921.
(31) Emsley, P., Lohkamp, B., Scott, W. G., and Cowtan, K. (2010) Features and development of Coot. *Acta Crystallogr. D66*, 486−501.
(32) DeLano, W. L. (2002) *The PyMol User's Manual*, DeLano Scientific, San Carlos, CA.
(33) Smoot, M. E., Ono, K., Ruscheinski, J., Wang, P. L., and Ideker, T. (2010) Cytoscape 2.8: New features for data integration and network visualization. *Bioinformatics 27*, 431−432.
(34) Kuratani, M., Ishii, R., Bessho, Y., Fukunaga, R., Sengoku, T., Shirouzu, M., Sekine, S. i., and Yokoyama, S. (2005) Crystal Structure of tRNA Adenosine Deaminase (TadA) from *Aquifex aeolicus*. *J. Biol. Chem. 280*, 16002−16008.
(35) Yuan, G., Bin, J. C., McKay, D. J., and Snyder, F. F. (1999) Cloning and characterization of human guanine deaminase. Purification and partial amino acid sequence of the mouse protein. *J. Biol. Chem. 274*, 8175−8180.
(36) Ko, T. P., Lin, J. J., Hu, C. Y., Hsu, Y. H., Wang, A. H., and Liaw, S. H. (2003) Crystal structure of yeast cytosine deaminase. Insights into enzyme mechanism and evolution. *J. Biol. Chem. 278*, 19111−19117.
(37) Seffernick, J. L., Dodge, A. G., Sadowsky, M. J., Bumpus, J. A., and Wackett, L. P. (2010) Bacterial Ammeline Metabolism via Guanine Deaminase. *J. Bacteriol. 192*, 1106−1112.
(38) Ingelfinger, J. R. (2008) Melamine and the Global Implications of Food Contamination. *N. Engl. J. Med. 359*, 2745−2748.
(39) Cook, A. F., Grossenbacher, H., and Hutter, R. (1984) Bacterial degradation of N-cyclopropylmelamine. The steps to ring cleavage. *Biochem. J. 222*, 315−320.
(40) Uddin, K. M., Almatarneh, M. H., Shaw, D. M., and Poirier, R. A. (2011) Mechanistic Study of the Deamination Reaction of Guanine: A Computational Study. *J. Phys. Chem. A 115*, 2065−2076.
(41) Sklenak, S., Yao, L., Cukier, R. I., and Yan, H. (2004) Catalytic Mechanism of Yeast Cytosine Deaminase: An ONIOM Computational Study. *J. Am. Chem. Soc. 126*, 14879−14889.
(42) Carter, C. W., Jr. (1995) The nucleoside deaminases for cytidine and adenosine: Structure, transition state stabilization, mechanism and evolution. *Biochimie 77*, 92−98.
(43) Chung, S. J., Fromme, J. C., and Verdine, G. L. (2005) Structure of Human Cytidine Deaminase Bound to a Potent Inhibitor. *J. Med. Chem. 48*, 658−660.
(44) Almog, R., Maley, F., Maley, G. F., MacColl, R., and Van Roey, P. (2004) Three-Dimensional Structure of the R115E Mutant of T4-Bacteriophage 2′-Deoxycytidylate Deaminase. *Biochemistry 43*, 13715−13723.